Lignocellulosic Flour-Reinforced Poly(hydroxybutyrate-co-valerate) Composites

Alain Dufresne, Danièle Dupeyre, Michel Paillet

Centre de Recherches sur les Macromolécules Végétales (CERMAV-CNRS), Université Joseph Fourier, BP 53, 38041 Grenoble cedex 9, France

Received 29 October 2001; accepted 6 May 2002

ABSTRACT: Residual lignocellulosic flour from spruce and ground olive stone was used as a natural filler in poly(hydroxybutyrate-co-valerate) (PHBV)-based composites. The morphology and the thermal properties of these composites were investigated by scanning electron microscopy and differential scanning calorimetry, respectively. Lignocellulosic fillers acted as nucleating sites for the crystallization of PHBV and strongly enhanced its degree of crystallinity. Dynamic mechanical analysis and tensile properties of these materials were also studied. A significant reinforcing effect was displayed by dynamic mechanical analysis at temperatures higher than the glass–rubber transition of the matrix. In addition, for low-particle-size spruce, a stabilization of the modulus was observed up to 500 K. High-strain tensile properties did not show any reinforcing effect. This apparent disagreement was explained by the poor adhesion between the hydrophilic lignocellulosic filler and the hydrophobic polymeric matrix. To validate this hypothesis, the experimental data were compared with predicted data involving the percolation concept. © 2002 Wiley Periodicals, Inc. J Appl Polym Sci 87: 1302–1315, 2003

Key words: fillers; composites; mechanical properties; cellulose; poly(hydroxyalkanoate)

INTRODUCTION

In recent years, increased interest in polymers that are environmentally friendly has been observed. This interest is due to the rapid rise in the use of polymers, particularly in the form of packaging materials, which has impacted negatively on the environment. However, the current price of these materials limits their use to a few exclusive applications in the fields of biomedicine and chiral synthesis.

Many aerobic and anaerobic bacterial species accumulate submicron inclusion bodies composed of poly(hydroxyalkanoates) (PHAs) under nutrient-limiting conditions with a sufficient supply of carbon.[1] These biopolymers are stored in intracellular inclusion bodies as an energy reserve.[2–4] PHAs are thermoplastic materials that have, in contrast to synthetic polymers, the fundamental advantage of being renewable resources that are not dependent on the supply of petroleum. The first and most prevalent PHA is poly(β-hydroxybutyrate) (PHB), a highly crystalline and brittle thermoplastic. This thermoplastic polyester constitutes a class of natural polymers with physical properties close to those of synthetic polymers. It displays the additional property of being completely biodegradable in carbon dioxide and water through natural microbiological mineralization, although it is water resistant. PHB can be produced from renewable raw materials, such as saccharides, alcohols, and low-molecular-weight fatty acids.[4] Despite these attractive properties, PHB is only used to a limited extent in industrial practice because of its brittleness and high cost.

ICI made a major advance in the production of PHB by patenting a procedure to produce copolymers of β-hydroxybutyrate and β-hydroxyvalerate.[5] This family of materials, known as PHBV or Biopol, has much improved properties over the original PHB, including reduced brittleness. This copolymer is more useful from a commercial point of view because its melting point can be lowered,[6] and its mechanical properties and thermoplastic characteristics can be greatly improved[7] by increasing the ratio of HV to HB repeating units.

The incorporation of filler in thermoplastics frequently contributes to obtaining a more competitive price and a general improvement in the load-bearing capability and thermal properties. The fiber reinforcement of matrices was initially developed using man-made fibers, such as glass, carbon, aramid, etc., taking advantage of their high tensile modulus. Over the last few years, a good deal of work has been dedicated to fibers of vegetable origin, with the possibility of replacing man-made fibers.[8–18] Numerous reasons support this choice: for examples, as material source, vegetable fibers are available throughout the world, they are renewable and biodegradable, and they can con-

Correspondence to: A. Dufresne (Alain.Dufresne@cermav.cnrs.fr).

Journal of Applied Polymer Science, Vol. 87, 1302–1315 (2003)

TABLE I
Codification, Particle Size, Apparent Density and Highest Possible Filling Level (HPFL) of Lignocellulosic Fillers

Filler	Filler codification	Particle size	Density ($g \cdot cm^{-3}$)	HPFL (wt%)
Spruce	S1	<250 μm	0.11–0.14	40
Spruce	S2	<50 μm	0.08–0.11	50
Olive stone	OS	100% $<$ 125 μm 60% $<$ 80 μm	0.45–0.50	70

tribute to a healthy ecosystem. The low cost and high performance of these fibers make them economically interesting for industrial applications. Concerning their intrinsic properties, these fibers have a specific weight that is half that of glass fibers and a tensile modulus for the ultimate fibril almost as high as that of aramid fibers. In addition, they reduce the abrasion of screw and barrel during extrusion. The low sensitivity against mechanical treatment results in longer fibers. Moreover, disposal by combustion of lignocellulosics-filled composites is easier compared with inorganic fillers systems. One inherent problem is the high variation of mechanical properties due to climatic and growing conditions, the different preparation methods, and water absorption.[11] Properties of fiber-reinforced composites depend on many factors, for instance fiber/matrix adhesion, volume fraction of fiber, fiber aspect ratio, fiber orientation, and stress-transfer efficiency of the interface.

The aim of this study has been to prepare and characterize composite materials composed of a PHB matrix and a cellulose flour reinforcing phase. This filler was expected to improve mechanical properties of PHB and to reduce the price of the finished article, preserving the biodegradability of the material. Attempts were also made to optimize filler–matrix interactions by plasma treatment of the filler.

EXPERIMENTAL

Materials

Polymeric matrix

PHBV was kindly supplied as a white powder by Monsanto Europe S.A. (Belgium) and was used as received. The PHBV had an HV content of 8% and a density of 1.256 g/cm^3 at room temperature. The melting temperature (T_m), determined experimentally by differential scanning calorimetry (DSC) at 10°C/min, was 150°C.

Filler

The experiments were carried out using three kinds of lignocellulosic fillers that were kindly supplied by Sociétě Parisienne des Poudres et Sciures (Argenteuil, France). They consisted of spruce *(Abies alba)* softwood residues and ground olive stone. The irregular brown particles were composed of cellulose, lignin, and hemicelluloses. The codification, particle size, and apparent density of the raw materials is shown in Table I.

Plasma modification

The lignocellulosic fillers were plasma-treated in a reactor at the Laboratoire d'Electrostatique et de Matériaux Diélectriques, Grenoble, France. The reactor was fitted with a localized microwave excitation and plasma confinement with a multipolar magnetic cage. Filler treatment involved the following sequence: a thin layer of lignocellulosic flour was placed in the glass reactor vessel and covered with a 1- or 20-μm pore size nylon net, depending on the filler particle size. This covering was used to prevent any contamination of the vacuum pump. The filler was treated for 30 min at 1600 W under nitrogen and hydrogen flows. The nitrogen and hydrogen pressures were 7×10^{-4} and 5.3×10^{-3} Torr, respectively, with the difference because of the higher diffusivity of hydrogen. For the lignocellulosic flour, obtained from ground olive stone, the plasma treatment was performed twice (2 times 30 min) because a 1-μm pore size nylon net was used. After plasma treatment, an argon and nitrogen flow under a few Torr of pressure was used for a few minutes to excite atoms with a noble gas. It is worth noting that the duration of the treatment was longer than what was reported in the literature[19–21] because both agitation and no nylon nets were used in these previous studies.

PHBV/lignocellulosic composites

A Brabender FDO 234H model mixer was used to mix and compound lignocellulosic fillers with the polymeric matrix. The compounding temperature was varied and optimized to obtain an easily processible homogeneous mixture and to avoid degradation of one of the constituent. Optimized compounding conditions were set at 170°C. PHBV was first melted at 170°C for 5 min using a rotor speed of 30 rpm. The lignocellulosic filler was added and mixed with PHBV at 170°C for an extra 5 min using the same rotor speed of 30 rpm. Composite compositions, with filler content ranging from 0 wt % to the highest as possible filling level (HPFL), were prepared. The HPFL corresponded

to the critical filler content beyond which the compound didn't show any cohesion and crumbled. This value was reported to depend on the filler type (see Table I). The volume fraction, ϕ_f, of filler was calculated from the weight fraction, w_f, by eq. 1:

$$\phi_f = \frac{w_f/\rho_f}{w_f/\rho_f + (1 - w_f)/\rho_m} \quad (1)$$

where ρ_f and ρ_m are the density of the lignocellulosic filler (~1.5) and of the matrix (~1.256), respectively.

After mixing, specimens for mechanical properties experiments were made by compression-molding the composites. The compounds were hot-pressed at 170°C with a CARVER Laboratory Press at 1.4 MPa (200 psi) for 3 min and at 13.8 MPa (2000 psi) for an extra 5 min. The films, between 0.4 and 0.8 mm thick, were slowly cooled at room temperature.

Methods

Scanning electron microscopy

Scanning electron microscopy (SEM) was performed with a JEOL JSM-6100 instrument to investigate both the morphology of the different kinds of fillers and the interface between the filler and the matrix. The specimens were frozen under liquid nitrogen, then fractured, mounted, coated with gold/palladium on a JEOL JFC-1100E ion sputter coater, and observed. SEM micrographs were obtained using 8 kV secondary electrons.

Differential scanning calorimetry

Differential scanning calorimetry (DSC) was performed with a Perkin-Elmer DSC7 fitted with a cooler system that used liquid nitrogen. The calorimeter was calibrated with an indium standard. Scans were performed at least 2 weeks after film formation to ensure stabilization of the degree of crystallinity and perfect reliability of measurements. At least three individual measurements were made to ensure reproducibility.

Each sample was heated from −80 to +220°C at a heating rate of 10 K/min (first scan corresponding to hot-pressed films). Subsequently, the samples were quenched to −80°C. The second scan heating curves (corresponding to quenched films) were then collected by heating from −80 to +220°C at 10 K/min. The melting (T_m) and crystallization (T_c) temperatures were taken as the peak temperature of the melting endotherm and crystallization exotherm, respectively, whereas the glass transition temperature (T_g) was taken as the inflection point of the specific heat increment at the glass–rubber transition.

Dynamic mechanical analysis (DMA)

The composite films, cut into strips 23 mm long and 4 mm wide, were analyzed with a DMTA Metravib SA Mécanalyseur operating with a forced oscillation pendulum. This apparatus provides the storage (G') and loss (G'') moduli of the complex shear modulus (G^*) and the internal friction coefficient ($\tan \delta = G''/G'$) as a function of frequency (isothermal conditions) or temperature (isochronal conditions). To remove most of water from the material, the specimens were immediately conditioned *in situ* in the spectrometer under vacuum, at room temperature, overnight before any measurement. It was checked that, under these conditions, a further conditioning did not modify the behavior. Measurements were performed under isochronal conditions from 200 to 520 K at 1 Hz, in the presence of liquid nitrogen. Between two measurements, the temperature was increased by steps of 4 K.

Tensile tests

The nonlinear mechanical behavior of lignocellulosic filler/PHBV composites was analyzed with an Instron 4301 testing machine in the tensile mode, with a load cell of 100 N capacity. The specimen was a thin rectangular strip (~20 × 5 × 0.5 mm). Tensile tests were performed at a strain rate of $d\varepsilon/dt = 1.7 \times 10^{-3}\ s^{-1}$ (cross-head speed = 1 mm/min) and at 25°C. The nominal strain ε can be determined by $\varepsilon = (L - L_o)/L_o$, where L and L_o are the length during the test and the length at zero time, respectively. The nominal stress σ was calculated by $\sigma = F/S_o$, where F is the applied load and S_o is the initial cross-sectional area. Stress versus strain curves were plotted and Young's modulus (E) was measured from the low strain region.

Ultimate mechanical properties were also characterized. The nominal ultimate stress, or nominal stress at break (tensile strength), $\sigma_b = F_b/S_o$, where F_b is the applied load at break, were reported for each tested sample. Ultimate elongation was characterized by the nominal ultimate strain, or nominal strain at break, $\varepsilon_b = \Delta L_b/L_o$, where ΔL_b is the elongation at break. The values reported in this study are the average of at least six measurements, and the reproducibility was very good.

RESULTS AND DISCUSSION

Morphological characterization

SEM was used to characterize both the structure (particle size, general aspect, and topography) of lignocellulosic fillers and the morphology of PHBV-based composite materials.

Filler structure

The SEM micrographs in Figure 1 show the structure of filler S1. This filler, obtained from spruce, occurs as

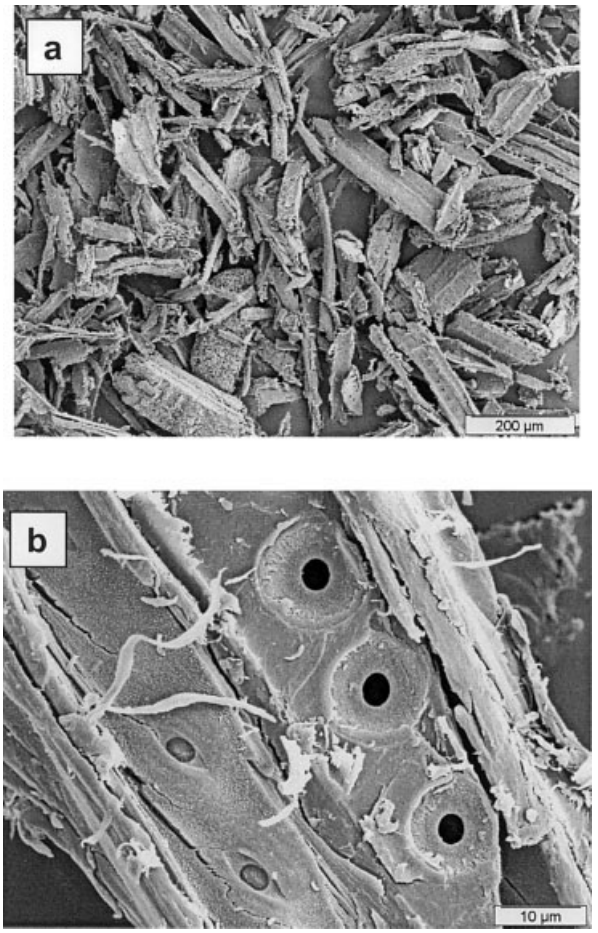

Figure 1 Scanning electron micrograph showing the filler S1 (high particle size lignocellulosic filler from spruce).

rod-like particles that are fiber fragments. This lignocellulosic filler displays a broad distribution in size, with lengths in the range 50–200 μm. The poor cohesion of the fibers is clearly observed in Figure 1b. The surface is made of numerous shrinkage folds that are composed of defibrillated cellulose microfibrils. Regular pits on the surface of the fiber, displayed in Figure 1b, allow sap circulation within the fiber.

The structure of filler S2, also obtained from spruce, is shown in Figure 2. The particle size is strongly reduced compared with that of filler S1. This lignocellulosic flour is composed of more or less regular lignocellulose fragments, with lengths in the range 10–30 μm. The structure of the lignocellulosic flour obtained from ground olive stone is completely different (Figure 3). It is constituted of well-individualized, compact, ovoid lignocellulose fragments with particle diameter sizes in the range 10–60 μm. Holes and concentric layers at the surface of these particles are clearly observed in Figure 3b.

Composite morphology

Scanning electron micrographs of freshly fractured surfaces of PHBV films filled with different amounts and types of lignocellulosic flour, with both untreated and treated fibers are shown in Figures 4–8. For each material, two different magnifications were used to display both the filler dispersion and interfacial adhesion. The micrograph in Figure 4 is of the surface of a fractured film obtained from the unfilled PHBV matrix, which is quite smooth and compact.

The SEM of the freshly fractured surface of a PHBV film filled with 20 wt % untreated filler S1 is shown in Figure 5. The filler is well dispersed in the matrix (Figure 5a). The absence of any physical contact between both components, shown in Figure 5b, clearly indicates that the interfacial adhesion between filler and matrix was poor. The fibers are pulled out from the matrix and practically intact. Fracturing the sample did not lead to breaking the filler. In addition, holes and spacing occur in the matrix as well as along the fiber, resulting in poor contact and inferior stress transfer between the phases. Similar results have been reported for cellulose-fiber-filled low-density polyethylene[22] or polypropylene.[23] Treating the filler S1 with plasma did not provide good apparent wetting as observed in the SEM of the freshly fractured surface of a PHBV film filled with 20 wt % treated filler S1

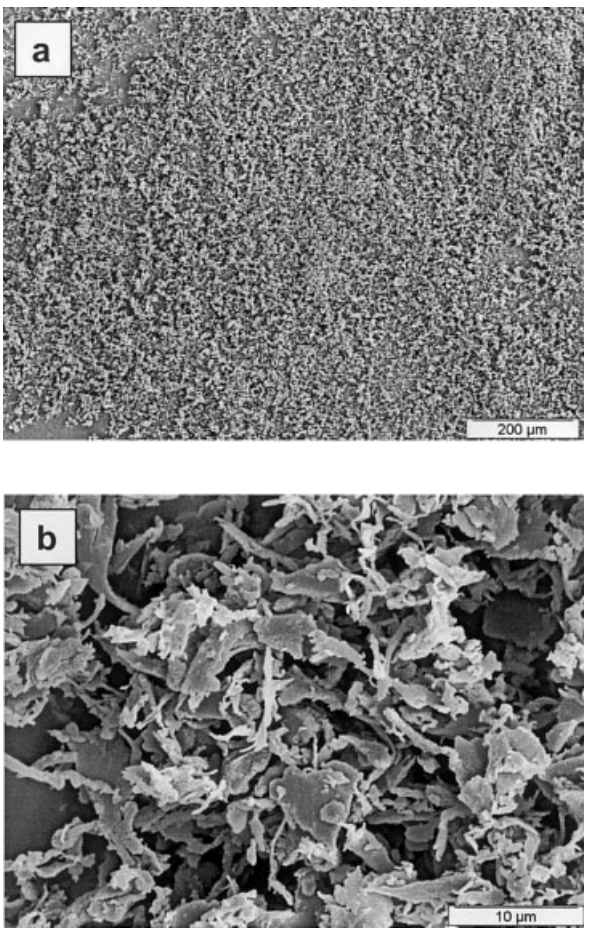

Figure 2 Scanning electron micrograph showing the filler S2 (low particle size lignocellulosic filler from spruce).

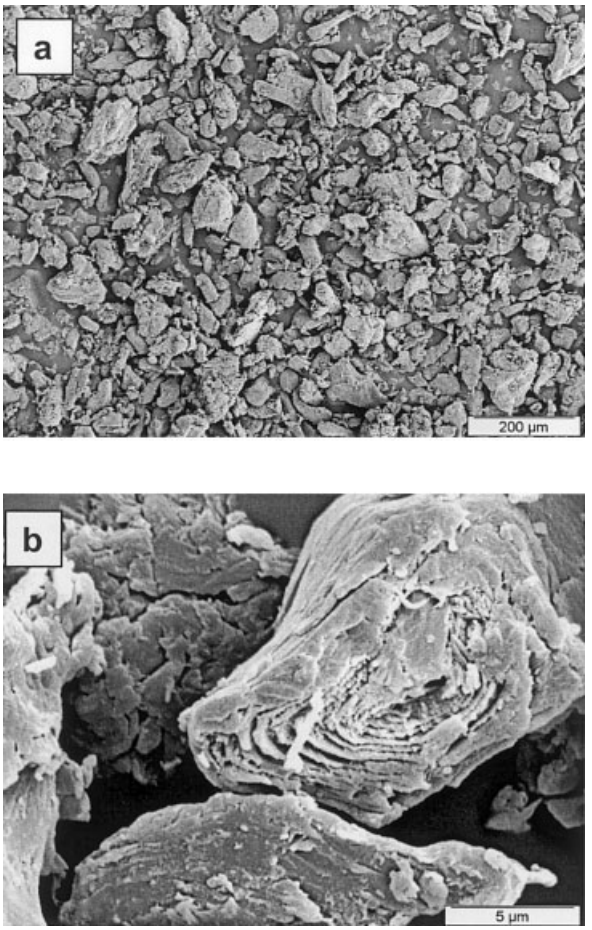

Figure 3 Scanning electron micrograph showing the filler OS (lignocellulosic filler from olive stone).

(Figure 6). Holes around the fillers and pull-out of fillers from the matrix during fracture are always observed.

The SEM of a freshly fractured surface of a PHBV film filled with 50 wt % untreated filler S2 is shown in Figure 7. Again, for this filler, the dispersion level within the matrix seems good. The interfacial adhesion between filler and matrix is difficult to determine, because of the size of the filler, but seems better than for filler S1 (Figure 7b). The SEM of a freshly fractured surface of a PHBV film filled with 50 wt % untreated filler OS is shown in Figure 8. Similar observations as those reported for filler S1 (Figure 5) can be seen. The filler is well dispersed in the matrix (Figure 8a) and the interfacial adhesion between filler and matrix is poor (Figure 8b). No significant difference with plasma treatment was reported.

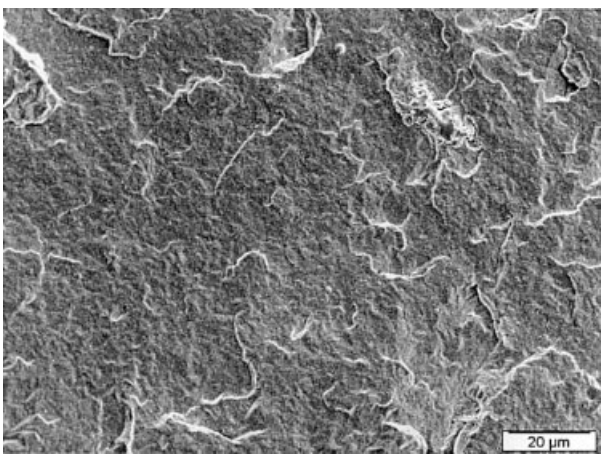

Figure 4 Scanning electron micrograph of a freshly fractured surface of an unfilled PHBV film.

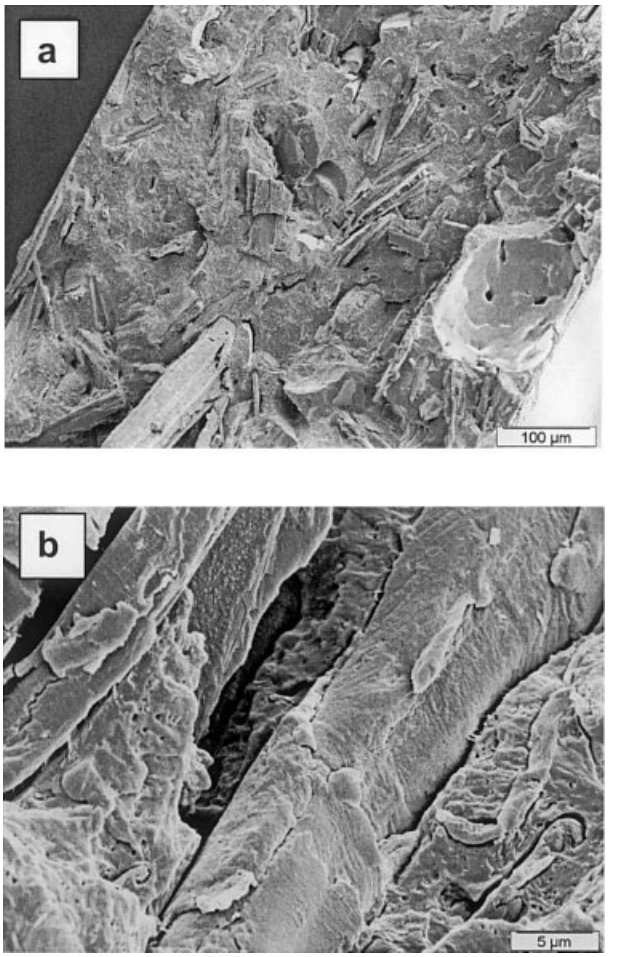

Figure 5 Scanning electron micrograph of a freshly fractured surface of a PHBV film filled with 20 wt % of filler S1.

Thermal behavior

DSC measurements were performed to characterize the thermal behavior of PHBV films filled with lignocellulosic flours. Two DSC traces of unfilled PHBV are shown in Figure 9. One scan corresponds to the DSC thermogram collected during the first heating scan (hot-pressed film), whereas the other one corresponds to the second heating scan (quenched film; see Experimental Section).

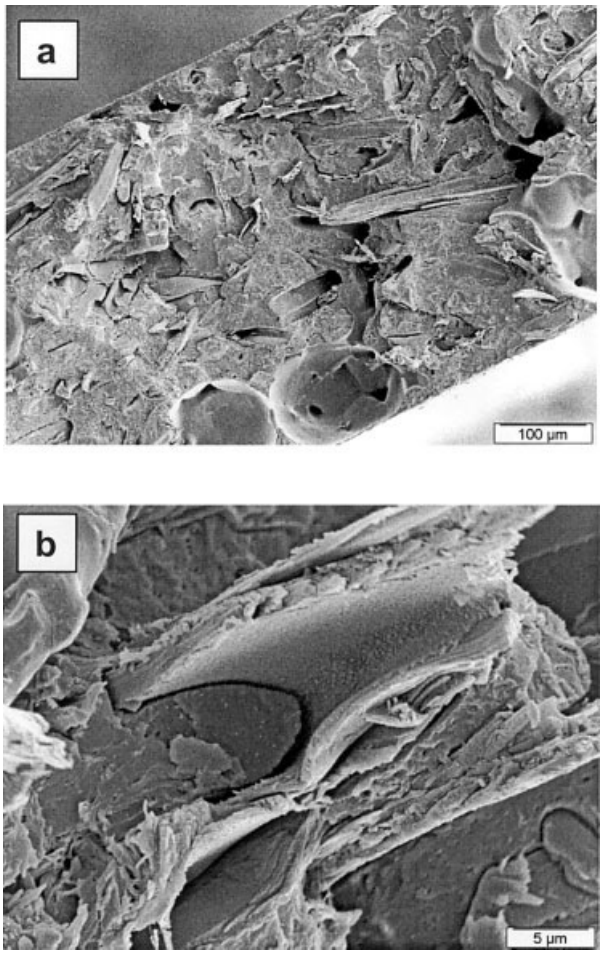

Figure 6 Scanning electron micrograph of a freshly fractured surface of a PHBV film filled with 20 wt % of plasma-treated filler S1.

The melting thermogram of unfilled hot-pressed PHBV exhibits an endothermal peak at ~150°C. This value is much lower than the one reported for PHB (~180°C)[24] because of the copolymerization with HV units. After quenching to −80°C, the second scan (Figure 9, quenched film) exhibits a specific heat increment around 0°C that is ascribed to the glass–rubber transition of PHBV. At higher temperature, an exothermal peak at ~75°C, corresponding to the crystallization of PHBV, is observed. The melting of these nonisothermally crystallized domains occurs at ~150°C.

The general appearance of the thermograms for both hot-pressed and quenched films of PHBV composites filled with lignocellulosic flours were similar (data not shown). The temperatures of the calorimetric transitions of the various compositions, taken from the DSC thermograms, are collected in Table II. The melting characteristics were determined from the first scan (hot-pressed films), whereas the crystallization and glass–rubber characteristics were obtained from the second scan (quenched films).

No significant shift was reported for the glass–rubber transition temperature of the amorphous domains of PHBV and the value range between −3.3 and −1.2°C. This temperature was not affected by either the filler loading or the plasma treatment of the filler. The crystallization temperature (T_c), taken as the position of the nonisothermal crystallization exothermic peak, was consistently lower for the composites than for the unfilled PHBV matrix, especially for filler S2 (low particle size spruce). It can be deduced that the lignocellulosic fillers act as nucleating agents, thus increasing the rate of crystallization. For fillers S1 and OS, this effect becomes more marked with increasing loading level. For filler S2, which presents the highest specific area, this trend tends to reverse with increasing loading level. For this filler, the process of nucleation may be in competition with polymer confinement effects caused by a higher amount of small size particles. The limited growth of PHBV spherulites most probably results from the lower amount of free volume for polymer crystallites to form. No clear trend is observed for plasma-treated lignocellulosic particles. The melting temperature (T_m) was almost

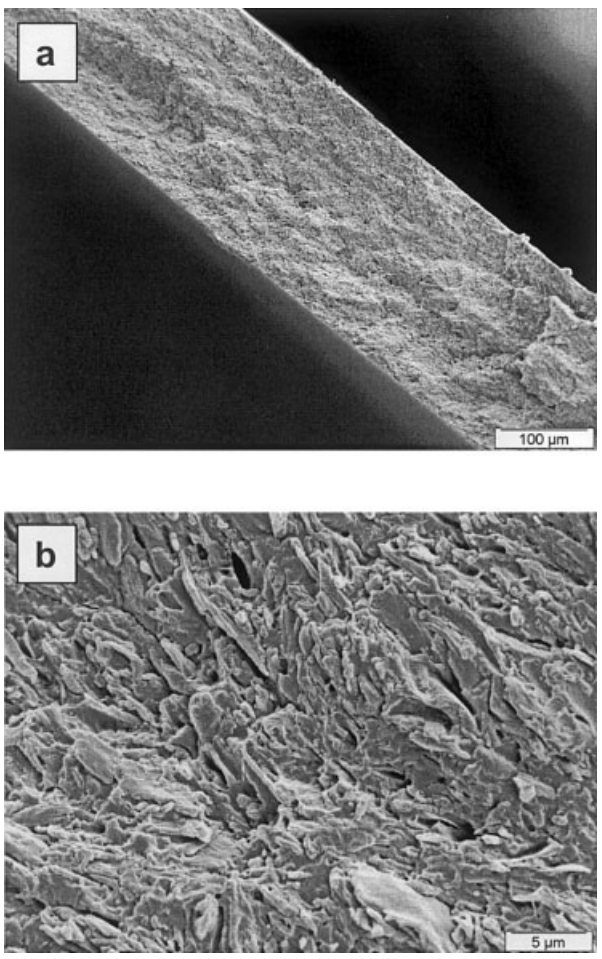

Figure 7 Scanning electron micrograph of a freshly fractured surface of a PHBV film filled with 50 wt % of filler S2.

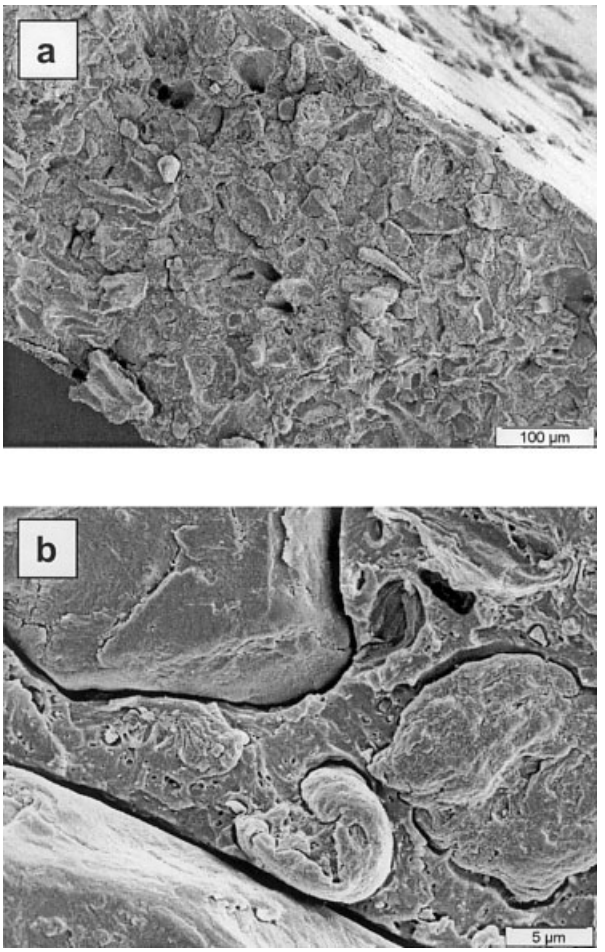

Figure 8 Scanning electron micrograph of a freshly fractured surface of a PHBV film filled with 50 wt % of filler OS.

unaffected by either the presence or the type of filler and was in the range 149.4–154.2°C regardless of the composition.

The enthalpies of crystallization, ΔH_c, and of fusion, ΔH_m, are also collected in Table II. It is worth noting that these values were calculated per gram of PHBV in the composite. Therefore, the enthalpy was obtained from the ratio of the apparent enthalpy and of the weight fraction of PHBV in the composite. Both ΔH_c and ΔH_m seem to globally increase as the filler content in the composite increases. This result can be most probably ascribed to an anchoring effect of the lignocellulosic filler. Lignocellulose probably acts as a nucleating agent for PHBV. This observation is in disagreement with previous results published by Gatenholm et al.[25] on wood cellulose-filled PHBV and those published by Luo and Netravali[26] on composites made from pineapple fibers and PHBV. These authors concluded that introducing cellulose neither affects the degree of crystallinity nor the crystallization kinetics of PHBV. On the contrary, Reinsch and Kelly[27] reported that short wood fibers acted as nucleating sites for the crystallization of PHBV and enhanced its crystallization rate. The results of the work Luo and Netravali[26] and Reinsch and Kelley[27] may have been influenced by the lignin of wood fiber. This explanation could be also the case for our findings in the present study. However, a similar effect was observed for poly(hydroxyoctanoate) (PHO), an elastomeric medium-chain-length PHA filled with tunicin whiskers consisting of pure animal cellulose.[28,29] In these last works, a possible transcrystallization phenomenon of PHO on the cellulose surface was reported.

No significant difference was observed between the three kinds of lignocellulosic flour, except for the crystallization in the presence of filler S1. For these filler-based composites, the enthalpy of crystallization was roughly unaffected by the loading level. Plasma treatment seems to increase the degree of crystallinity for filler S1, but the opposite trend is reported for filler OS.

Mechanical behavior

Dynamic mechanical analysis (linear conditions)

Dynamic mechanical measurements were performed on PHBV composites filled with lignocellulosic to display the effect of the filler content, the plasma treatment, and the filler type. The curves of log (G'/Pa) (storage shear modulus) versus temperature at 1 Hz are displayed in Figures 10a, 10b and 10c, for fillers S1, S2, and OS, respectively. For low temperatures, it was difficult to observe any change in the modulus with variation in the filler loading. As is well known, the exact determination of the glassy modulus depends on the precise knowledge of the sample dimensions. To minimize this effect, the elastic shear modulus, G' at 200 K was normalized at 1 GPa for all the samples. This procedure can be justified by the fact that the difference between the elastic modulus of the glassy polymer and lignocellulosic filler was not high enough to easily appreciate any change.

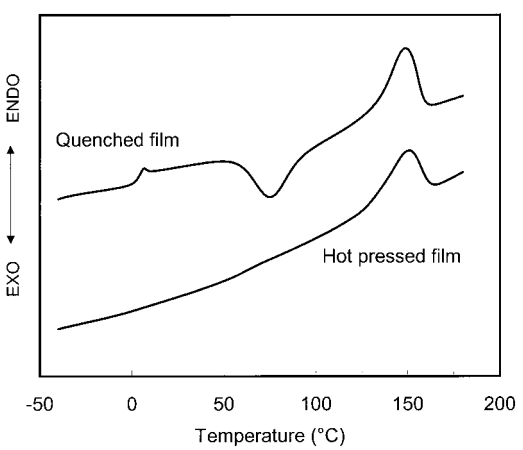

Figure 9 DSC thermograms of hot-pressed PHBV and PHBV after melt quenching.

TABLE II
Temperatures of the Calorimetric Transitions of Lignocellulosic Flour-Filled PHBV using Data Obtained from the DSC Curves[a]

PHBV	Flour content (wt %)	T_g (°C)	ΔCp (J · g^{-1} · K^{-1})	T_c (°C)	ΔH_c (J · g^{-1})	T_m (°C)	ΔH_m (J · g^{-1})
PHBV	0	−1.9	0.7	51.8	−49.8	151.3	76.5
PHBV + S1	20	−1.7	0.5	42.4	−42.5	154.2	83.3
	20T[b]	−1.9	0.6	42.1	−52.5	151.1	105.3
	40	−1.6	0.5	39.0	−46.7	153.4	107.7
PHBV + S2	20	−1.8	0.6	38.8	−41.6	152.7	82.8
	40	−1.2	0.5	39.8	−71.5	152.8	114.2
	50	−2.1	0.6	40.6	−81.2	151.0	122.6
PHBV + OS	20	−2.4	0.7	46.0	−55.3	151.1	94.9
	20T[b]	−2.3	0.6	49.3	−54.1	152.1	75.9
	40	−2.3	0.6	44.5	−72.0	152.5	108.3
	50	−2.4	0.6	42.6	−87.8	150.9	134.0
	70	−3.3	0.7	42.1	−145.7	149.4	214.7

[a] Glass–rubber transition temperature (T_g) and associated heat increment (ΔC_p); crystallization temperature (T_c) and associated heat of crystallization (ΔH_c); and melting temperature (T_m) and associated heat of fusion (ΔH_m).
[b] Plasma-treated Filler.

The curve corresponding to the nonreinforced PHBV matrix is typical of semicrystalline thermoplastic behavior. The storage modulus remains practically constant up to a temperature of ~270 K. At higher temperatures, a slight decrease in the elastic shear modulus was observed, corresponding to the glass–rubber transition. This slight modulus drop corresponds to energy dissipation displayed in a relaxation process, where tan ϕ passes through an ill-defined maximum (not shown). This relaxation process, labeled α, involves cooperative motions of long amorphous chain sequences. The rubbery modulus is known to depend on the degree of crystallinity of the material. The crystalline regions act as physical crosslinks for the elastomer. In this physically crosslinked system, the crystalline regions would also act as filler particles because of their finite size, which would increase the modulus substantially. In the terminal zone, corresponding to the melting of crystalline domains (~425 K), the elastic shear modulus becomes lower and lower with temperature, and the experimental setup fails to measure the change.

The effect of the addition of untreated lignocellulosic flours to the host PHBV polymer is displayed in Figure 10. The three kinds of filler used were S1, S2, and OS flours. Regardless of the nature of the flour, the modulus drop at the glass–rubber transition decreases, and therefore the rubbery modulus increases, with increasing filler loading. For instance, the relaxed modulus increases from 120 MPa for the unfilled matrix up to 285, 265, and 400 MPa for the 40 wt % S1, 50 wt % S2, and 70 wt % OS-filled composite, respectively, at 350 K. This increase in rubbery modulus can be ascribed to both a reinforcing effect of the filler and/or to the increase of the degree of crystallinity previously reported from DSC measurements. These two factors could influence the modulus in the same way and are difficult to separate. At higher temperature, most of the composites display an irreversible modulus drop corresponding to the melting of the crystalline domains of PHBV, except for the sample filled with 50 wt % of filler S2 (Figure 10b, low particle size spruce). For this material, the storage shear modulus remains roughly constant at ~3 MPa up to 500 K, a temperature at which cellulose starts to decompose. This phenomenon can be most probably ascribed to the presence of strong interactions between the lignocellulosic fillers, such as hydrogen bonds, which lead to the formation of a rigid network for this concentration and this kind of filler. These interactions hold only for filler S2 that displays the higher specific area. A similar shear modulus stabilization at $T > T_m$ is also weakly observed up to 440 K for the composite reinforced with 70 wt % filler OS. At this temperature, the sample was broken near the jaws most probably because of damage induced by the tightening. Indeed, for the same composition, the breakup of the sample corresponding to the end of the plateau occurred at different temperatures from one experiment to another. Because the matrix becomes a viscous liquid from T_m, this phenomenon can only be explained by the formation of a stable rigid phase. So, the degradation temperature of this rigid phase can be >440 K. Because storage modulus measurements at $> T_m$ are very difficult to reproduce, differences observed between the different kinds of fillers may not be real.

The evolution of the storage shear modulus of 20 wt % plasma-treated composites filled with lignocellulosic flour as a function of temperature is displayed as a continuous line in Figures 10a and 10c, for filler S1 and OS, respectively. Compared with the untreated filler, the rubbery modulus of the composites is higher. Indeed, the relaxed modulus of the composite filled with 20 wt % plasma-treated filler is similar to that of the composite filled with 40 wt % untreated filler. For filler S1, the reinforcing effect of the treated

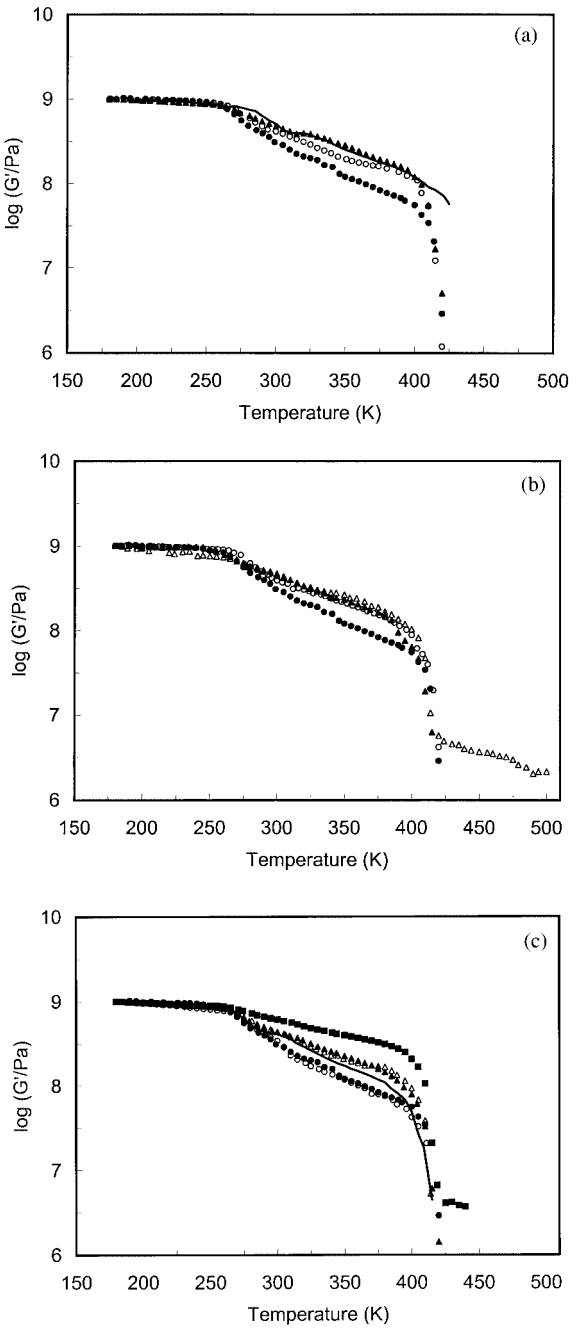

Figure 10 Storage shear modulus G' versus temperature at 1 Hz for (a) S1, (b) S2, and (c) OS lignocellulosic-flour-filled PHBV. Key: (●) unfilled matrix; (○) 20 wt % filled materials; (continuous line) 20 wt % plasma-treated filled materials; (▲) 40 wt % filled materials; (△) 50 wt % filled materials; and (■) 70 wt % filled materials.

filler should be minimized because an increase in the degree of crystallinity of the matrix was reported on treatment. On the contrary, an actual reinforcing effect of treated filler OS is reported, because a decrease of the degree of crystallinity of the matrix was observed on treatment.

To compare the reinforcing effect of the various types of filler, the rubbery modulus at 350 K was plotted against flour content in Figure 11. For a given loading level, the reinforcing effect is higher for spruce flour compared with olive stone flour. There is no significant change with the particle size of spruce flour. The rubbery modulus data of plasma-treated, filler-based composites are labeled with the letter "T".

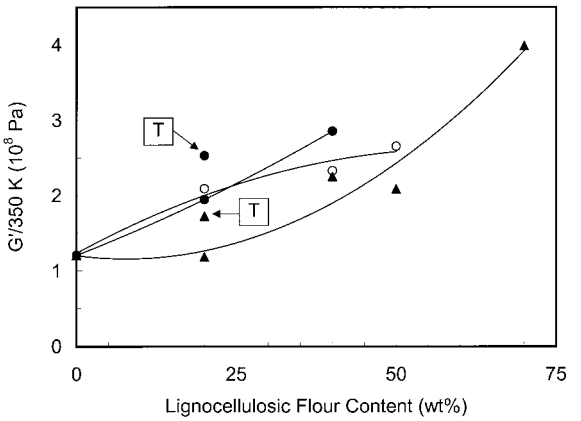

Figure 11 Storage shear modulus G' at 350 K versus filler content for lignocellulosic-flour-filled PHBV. Key: (●) filler S1; (○) filler S2; and (▲) filler OS. The data of plasma-treated filler-based composites are labeled with the letter "T" and the solid lines serve to guide the eye.

High-strain behavior (nonlinear conditions)

The effect of filler loading on the high-strain behavior of lignocellulosic flour/PHBV composites was investigated up to the break. Typical stress versus strain curves for filler S2 reinforced PHBV composite at 25°C are reported in Figure 12. At this temperature, PHBV displays a ductile behavior and breaks at $\varepsilon_b \sim 17\%$. With increasing filler content, the material becomes more brittle. The slope in the vicinity of $\sigma = \varepsilon = 0$ (i.e., determined for $\varepsilon < 1\%$) is equal to the tensile or Young's modulus, which is known to depend on both

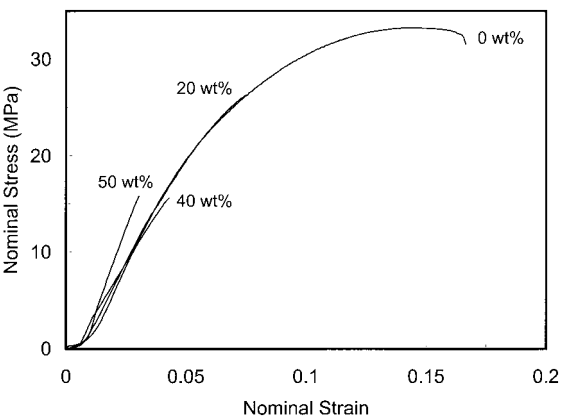

Figure 12 Typical stress versus strain curves of lignocellulosic-flour-S2-reinforced PHBV composites at 25°C ($d\varepsilon/dt = 1.7 \times 10^{-3}$ s^{-1}). The lignocellulosic filler contents are indicated in the figure.

TABLE III
Mechanical Properties of Lignocellulosic Flour-Filled PHBV using Data Obtained from Tensile Tests

PHBV	Flour content (wt %)	E (MPa)	σ_b (MPa)	ε_b (%)
PHBV	0	560	32.0	17
PHBV + S1	20	360	19.6	9.1
	20T[b]	390	17.7	6.6
	40	460	20.2	6.6
PHBV + S2	20	440	24.0	6.9
	40	450	17.4	5.5
	50	670	13.9	3.1
PHBV + OS	20	460	18.6	7.7
	20T[b]	350	16.5	8.9
	40	420	14.0	6.6
	50	420	13.2	5.3
	70	320	9.1	4.5

[a] Tensile modulus (E), stress at break (σ_b), and elongation at break (ε_b).
[b] Plasma-treated filler.

the strain rate and the temperature. These results, as well as the stress and strain at break for the three kinds of fillers are reported in Table III. It is observed that the mechanical properties of the unfilled PHBV matrix are as follow : E = 560 MPa, σ_b = 32 MPa, and ε_b = 17%.

No reinforcing effect of the lignocellulosic filler is evident because the Young's modulus is almost constant and seems, in fact, to roughly decrease with filler content. This result seems to disagree with the reinforcing effect of lignocellulosic fillers indicated by dynamic mechanical analysis. However, it is worth noting that because dynamic mechanical analysis involves weak stresses, the adhesion between the filler and the matrix is not damaged. Under higher stress, as used for tensile tests, adhesion is involved. The result is therefore an indication of the lack of intimate adhesion between both components. This lack of adhesion leads to numerous irregularly shaped microvoids or microflaws in the composite structure. Because of these microflaws, the transfer of stress from the matrix to the filler is poor, and the mechanical properties of the filler are not fully utilized. Assuming this point, the decrease of the modulus observed with increasing filler loading in tensile tests remains nevertheless surprising because DSC measurements show that the higher the filler content, the higher the degree of crystallinity. This increase in the degree of crystallinity should have an effect on the mechanical behavior of the composite and should increase the tensile modulus substantially. It seems therefore that the poor adhesion between the filler and the matrix has a greater effect on the mechanical properties than the increase of the degree of crystallinity.

The evolution of tensile strength as a function of lignocellulosic filler content is shown in Figure 13a. The addition of the filler in the PHBV matrix affects the tensile strength of the composite. The tensile strength decreases more or less regularly from 32 MPa for the unfilled system down to 20.2, 13.9, and 9.1 MPa for the 40 wt % S1-, 50 wt % S2-, and 70 wt % OS-filled composites, respectively. This phenomenon is due to a

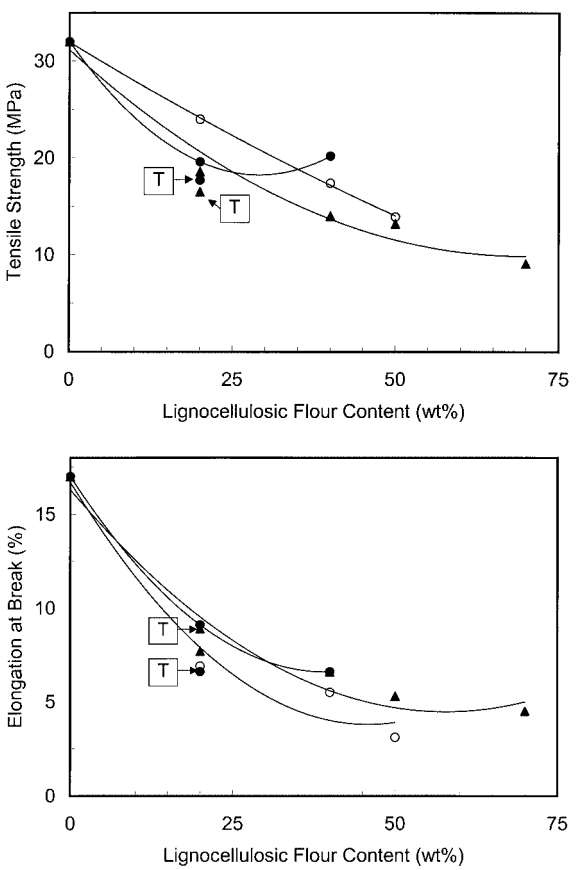

Figure 13 Tensile strength (a) and elongation at break (b) of lignocellulosic-flour-reinforced PHBV composites. Key: (●) filler S1; (○) filler S2; and (▲) filler OS. The data of plasma-treated filler-based composites are labeled with the letter "T" and the solid lines serve to guide the eye.

crazing effect or to a dewetting effect in which the adhesion between the filler and the matrix is destroyed, leading to a weakening of the interface strength. This result is in agreement with morphological observations by SEM. The poor interfacial adhesion of the fillers to the polymer matrix may explain this reduction, because the effective transfer of stress between matrix and filler requires adequate interfacial bonding.[30,31]

The evolution of the elongation at break versus filler content is shown in Figure 13b. PHBV displays ductile behavior at room temperature, with elongation at break of 17%. Fillers cause a decrease in elongation at break, and PHBV-based composites display brittle behavior at high filler loading; it breaks for $\varepsilon < 10\%$ when only 20 wt % of fillers were included in PHBV. This well-known decrease in elongation at break with rigid fillers arises from the fact that the actual elongation experienced by the polymer matrix is much higher than the measured elongation of the specimen. In addition, the increase of the degree of crystallinity with lignocellulosic filler loading leads to a decrease of the elongation at break. A distinct difference is not observed either of the various types of filler or when the filler is plasma-treated.

Modeling of the tensile behavior

The modeling of the tensile properties of the materials and comparison with experimental data are powerful tools to relate the microstructure and the mechanical behavior of PHBV filled with lignocellulosic flour. In multiphase polymer systems, the relationship between the elastic moduli, the composition of the two components, and the morphologies (or geometrical arrangement of each phase) has been extensively studied. Different models can be used to predict the elastic behavior of two-phase systems.[24,32–41] Most theories assume that adhesion between phases is perfect and that the sample is macroscopically homogeneous and isotropic. In fact, it has been shown that the polymer matrix used in this study is a two-phase system, with PHBV being a semicrystalline polymer. Because it is very difficult to derive a model for such composite systems, it is of interest to consider the following hypothesis. At a temperature between their T_g and their melting point, semicrystalline polymers are often considered to be a soft matrix reinforced by crystallites. Their mechanical behavior as well as T_g of their amorphous phase mainly depends on the crystallinity ratio, the average crystallite size, and the interface between the crystalline phase and the amorphous phase. However, at the scale of the average size of matrix domains in our composites, if no specific orientation occurs during processing, the behavior of most semicrystalline polymers can be considered homogeneous and isotropic. Accordingly, for modeling the mechanical behavior of the composites, they may be considered as two-phase systems, with each phase being homogeneous and having the same macroscopic behavior as PHBV or cellulose.

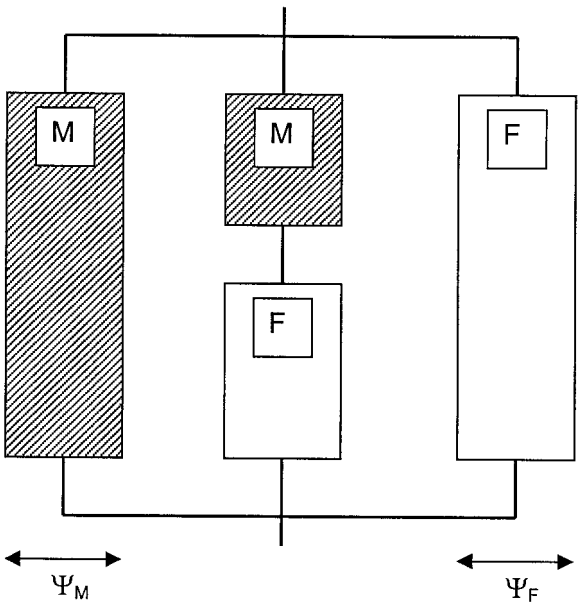

Figure 14 Schematic diagram for the "three branch" series-parallel model (3B).

In previous works, the series–parallel model proposed by Takayanagi,[33] in which the concept of percolation was introduced,[38] gave successful results when applied to cellulose/PA66,[39] cellulose/PA6,69,[40] chitosan/PA6,[41] and PHB/PHO blends.[24] The Takayanagi prediction is a phenomenological model that consists of a mixing rule between the two simplest models involving connections of the components in series (Reuss prediction) or in parallel (Voigt prediction). However, it was shown that for blends involving semicrystalline polymers, a better prediction of the mechanical behavior can be performed by using a "three branch" model rather than the classical "two branch" model.[24,39–41]

A schematic diagram of the "three branch" model (which will be referred to as the 3B model hereafter) is given in Figure 14, where M and F refer to the matrix and the filler, respectively. Under a tensile situation the predicted modulus, E, of the 3B model is given by (see ref. 24 or 39 for the full calculation):

$$E = \Psi_M E_M + \frac{(1 - \Psi_M - \Psi_F)E_M E_F}{\Psi_F E_M + (1 - \phi_F)E_F} + \Psi_F E_{FP} \quad (2)$$

where E_M, E_F, and E_{FP} correspond to the tensile modulus of the matrix, embedded lignocellulosic filler, and percolating filler, respectively; Ψ_M and Ψ_F are the volume fraction of the matrix and filler phase, respectively, which has percolated (i.e., which presents a continuity within the film); and $\phi_F = \phi_M - 1$, is the

volume fraction of the filler (ϕ_M being the volume fraction of the matrix). Considering ϕ_{Mc} and ϕ_{Fc} as the critical volume fraction of the matrix and the filler, respectively, at the percolation threshold, and b_M and b_F as the corresponding critical exponents, $\Psi_{M(F)}$ can be written as:

$$\Psi_{M(F)} = \phi_{M(F)} \left[\frac{\phi_{M(F)} - \phi_{M(F)c}}{1 - \phi_{M(F)c}} \right]^{b_{M(F)}} \quad \text{for } \phi_{M(F)} > \phi_{M(F)c}$$
$$\Psi_{M(F)} = 0 \quad \text{for } \phi_{M(F)} < \phi_{M(F)c} \tag{3}$$

Equation 3 is consistent with the fact that Ψ_M and Ψ_F should be equal to 1 when ϕ_M and $\phi_F = 1$, respectively.

Although it is difficult to determine ϕ_{Mc}, ϕ_{Fc}, b_M, and b_F (eq. 3) because they depend on many parameters (e.g., the geometry and the spatial distribution of each phase). we have considered that $\phi_{Mc} = \phi_{Fc} = 1 - \phi_{max}$, where ϕ_{max} is the maximum volume fraction of rigid isoradius spheres, so that $\phi_{Mc} = \phi_{Fc} \approx 0.25$. The critical exponents b_M and b_F of the probability to obtain an infinite cluster are ~0.4 for the random sites percolation model.[42,43] The application of this model requires knowledge of the experimental mechanical behavior of the pure parent components, PHBV and lignocellulosic filler.

The tensile modulus, E, of PHBV composites filled with lignocellulosic flour was predicted with the 3B model. For both the experimental and predicted data, E is plotted on a linear scale versus lignocellulosic flour content in Figure 15. The mechanical characteristics of the various components were calculated as follows. The modulus, E_M, of the unfilled matrix was experimentally measured (560 MPa). As the filler content was increased, it was observed by DSC that the degree of crystallinity of the matrix increased, thus changing the tensile modulus of the PHBV. To account for this effect, the evolution of the heat of fusion versus filler content was fitted with a polynomial second-order equation. The fitting equations corresponding to the three types of fillers are given in Table IV. This information allows one to know the heat of fusion for any composition. To deduce the tensile modulus of the matrix from the heat of fusion, a rough assumption was made. It was assumed that E varies linearly with the degree of crystallinity of the matrix. One point of this linear regression is known; that is, the experimental data for the unfilled matrix ($\Delta H_m = 76.5\ J \cdot g^{-1}$; $E_M = 560$ MPa). In addition, it is well known that the rubbery modulus of any fully amorphous polymer is ~1 MPa ($\Delta H_m = 0\ J \cdot g^{-1}$; $E_M = 1$ MPa). The fitting equation, given in Table IV, allows the determination of the tensile modulus for any degree of crystallinity and therefore for any composition. The value of E_F was taken as 10 GPa, which corresponds to the experimental value obtained for steam-exploded poplar wood[44] and cotton.[45] The modulus E_{FP} of the percolating filler network could be experimentally measured from a tensile test performed on a lignocellulosic flour-pressed film. However, such a film is difficult to process because it does not display any

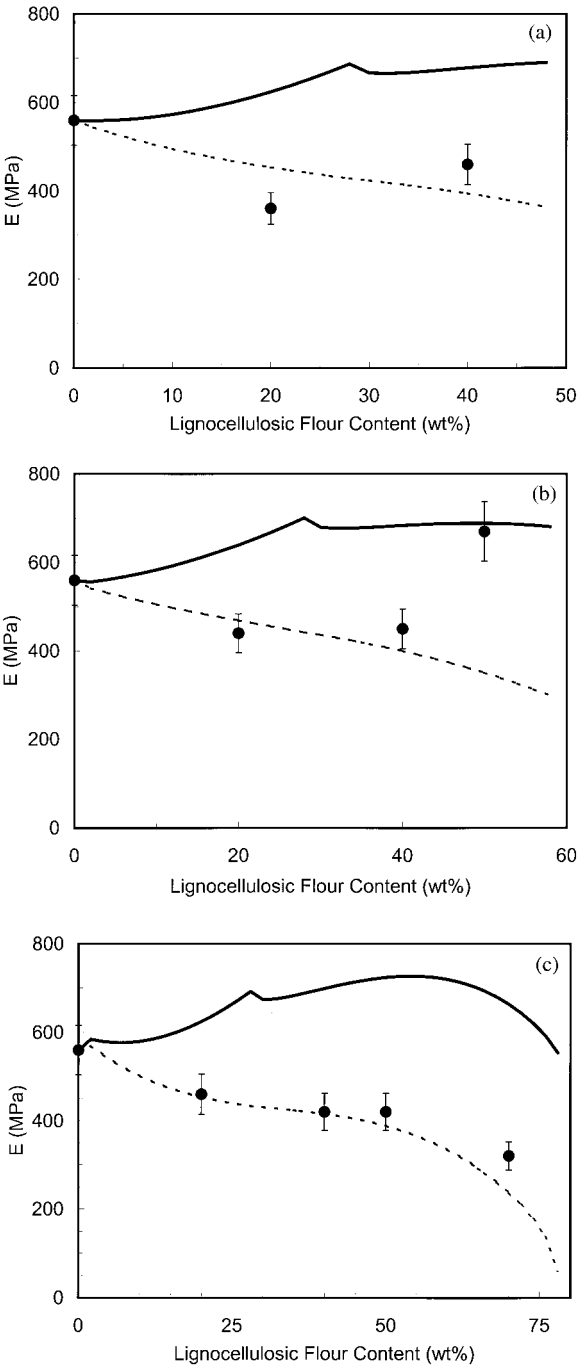

Figure 15 Experimental and predicted data for the tensile modulus of lignocellulosic flour-reinforced PHBV composites [(a) S1, (b) S2, and (c) OS] versus lignocellulosic filler content. Key: (●) experimental data; (continuous line) predicted data for the case of complete 3B model; and (dashed line) predicted data for the case of nonadhesion between both phases.

TABLE IV
Parameters used for the 3B Model

Parameter	Filler	Value
Fitting equation for ΔH_m vs. w_F	S1	$\Delta H_m = 220 w_F^2 - 10 w_F + 76.5$
	S2	$\Delta H_m = 154 w_F^2 + 22.5 w_F + 75.5$
	OS	$\Delta H_m = 349 w_F^2 - 58 w_F + 81$
Fitting equation for E_M vs. ΔH_m	All	$E_m = 7.3\ \Delta H_m + 1$
E_F	All	10 GPa
E_{FP}	All	28 MPa

cohesion and it crumbles. Therefore, E_{FP} was estimated from the storage shear modulus (G_{FP}) that was experimentally measured at high temperature ($T > T$m) for the 50 wt % filler S2-filled PHBV composite. Indeed, the high temperature modulus stabilization was assigned to interactions between the lignocellulosic fillers. Because the matrix becomes a viscous liquid from T_m, this phenomenon can only be explained by the formation of a stable rigid phase; that is, $\Psi_F \times G_{FP} \sim 3$ MPa, that is to say $G_{FP} \sim 11$ MPa or $E_{FP} \sim 28$ MPa, assuming $\nu_F \sim 0.3$. In fact, this value is very low and will not have any significant effect on the prediction of the composite modulus. However, it accounts for the modulus stabilization at high temperature. The parameters involved in the 3B model are shown in Table IV.

Three variations of the 3B model were used. The behavior of the material in the case of weak adhesion (i.e., excluding the second term in eq. 2, which corresponds to the two phases connected in series) is reported as a dashed line in Figure 15. The tensile modulus of the cellulose-filled PHBV was also predicted in the case of breakage of the percolating filler phase (i.e., excluding the third term in eq. 2, which corresponds to the continuous filler phase), and in the case of both weak adhesion and breakage of the percolating cellulose phase. These predicted data are not reported in Figure 15 because they are the same as the data for the complete 3B model (for the case of breakage of the percolating filler phase) and the data for the case of weak adhesion (for the case of both weak adhesion and breakage of the percolating cellulose phase). The similarity in these data is because the modulus E_{FP} of the percolating filler network is very low and negligible, at least up to the T_m of the matrix.

We ascertained that the experimental data, except for the 50 wt % filler S2-based composite, were poorly fit by the 3B model (continuous line in Figure 15). This 50 wt % filler S2-based composite displayed a specific behavior when characterized by dynamic mechanical analysis. A thermal stabilization of the modulus was observed for this specimen at $T > T_m$ up to 500 K. For all other composites, the prediction from the 3B model is systematically higher than the experimental modulus. The good agreement between experimental and predicted data in the case of weak adhesion (dashed line in Figure 15) is an indication of poor adhesion between cellulose and PHBV. This expected result is due to the hydrophobic nature of PHBV and hydrophilic nature of cellulose.

CONCLUSIONS

Compounding and molding lignocellulosic flour with PHBV formed composite materials. Three types of filler were used; namely, low- and high-particle-size spruce and ground olive stone. One of the objectives of the study was to decrease the cost of PHBV by preserving its biodegradability. The highest filling level was obtained with ground olive stone (70 wt %), which has the highest apparent density. SEM was used to characterize both the structure of the fillers and the morphology of composite materials. A poor interfacial adhesion between the filler and the matrix was observed, even when the lignocellulosic flour was plasma-treated. No significant shift of either the glass–rubber transition or melting temperatures of PHVB was reported following filler loading or plasma treatment. However, a decrease of the crystallization temperature and a strong increase of the enthalpy of fusion were observed in the presence of the lignocellulosic flour. It was suggested that the lignocellulosic fillers most probably act as nucleating sites for the crystallization of PHBV. A significant increase of the rubbery modulus, determined by dynamic mechanical analysis, was ascribed to a reinforcing effect of the filler and/or the increase of the degree of crystallinity following addition of filler. A stabilization of the modulus at temperatures higher than the melting temperature of PHBV was observed up to 500 K for the 50 wt % low-particle-size spruce composite. This result is most probably due to strong interactions between lignocellulosic particles and to the formation of a rigid percolating phase within the matrix. High-strain tensile tests revealed the poor mechanical properties of the composites, which were ascribed to poor interfacial adhesion between the filler and the matrix. The experimental data were compared with predicted data involving the percolation concept. Despite some rough approximation, a good agreement between both sets of data was reported. This agreement accounts for

the effect of the lack of adhesion between the filler and the matrix.

The authors gratefully acknowledge Société Parisienne des Poudres et Sciures (Argenteuil, France) for providing lignocellulosic fillers, Monsanto Europe S.A. (Belgium) for providing poly(hydroxybutyrate-co-valerate), Mrs. K. Lagarde for her help in film processing, and Mr. Y. Arnal of Laboratoire d'Electrostatique et de Matériaux Diélectriques for plasma treatment.

References

1. Hocking, P.J.; Marchessault, R.H. In Biopolymers from Renewable Resources; Kaplan, D.L., Ed.; Springer-Verlag: Berlin, Heidelberg, 1998; Chapter 9, pp. 220–248.
2. Dawes, E.A.; Senior, P.J. Adv Microbiol Physiol 1973, 10, 203.
3. Erson, A.J.; Dawes, E.A. Microbiol Rev 1990, 54, 450.
4. Doi, Y. Microbial Polyesters; VCH Publishers: New York, 1990.
5. Holmes, P.A.; Wright, L.F.; Collins, S.H. Eur Patent No EP 52459, 1982.
6. Bluhm, T.L.; Hamer, G.K.; Marchessault, R.H.; Fyfe, C.A.; Veregin, R.P. Macromolecules 1986, 19, 2871.
7. Byrom, D. Trends Biotechnol 1987, 5, 246.
8. Klason, C.; Kubat, J.; Strömvall, H.E. Int J Polym Mater 1984, 10, 159.
9. Zadorecki, P.; Michell, A.J. Polym Compos 1989, 10, 69.
10. Maldas, D.; Kokta, B.V. Int Trends Polym 1993, 1, 174.
11. Maldas, D.; Kokta, B.V.; Daneault, C. J Appl Polym Sci 1989, 38, 413.
12. Raj, R.G.; Kokta, B.V.; Groleau, G.; Daneault, C. Plast Rubber Process Appl 1989, 11, 215.
13. Raj, R.G.; Kokta, B.V.; Maldas, D.; Daneault, C. Polym Compos 1988, 9, 404.
14. Glasser, W.G.; Taib, R.; Jain, R.K.; Kander, R. J Appl Polym Sci 1999, 73, 1329.
15. Raj, R.G.; Kokta, B.V.; Groleau, G.; Daneault, C. Polym Plast Technol Eng 1990, 29, 339.
16. Bledzki, A.K.; Gassan, J. Prog Polym Sci 1999, 24, 221.
17. Sanadi, A.R.; Prasad, S.V.; Rohatgi, P.K. J Sci Ind Res 1985, 44, 437.
18. Sanadi, A.R.; Rowell, R.M.; Caulfield, D.F. Polym News 1996, 20, 7.
19. Felix, J.; Gatenholm, P.; Schreiber, H.P. J Appl Polym Sci 1994, 51, 285.
20. Felix, J.; Carlsson, C.M.G.; Gatenholm, P. J Adhesion Sci Technol 1994, 8, 163.
21. Deslandes, Y.; Pleizier, G.; Poiré, E.; Sapieha, S.; Wertheimer, M.R.; Sacher, E. Plasma Polym 1998, 3, 61.
22. Hedenberg, P.; Gatenholm, P. J Appl Polym Sci 1995, 56, 641.
23. Anglès, M.N.; Salvadó, J.; Dufresne, A. J Appl Polym Sci 1999, 74, 1962.
24. Dufresne, A.; Vincendon, M. Macromolecules 2000, 33, 2998.
25. Gatenholm, P.; Kubat, J.; Mathiasson, A. J Appl Polym Sci 1992, 45, 1667.
26. Luo, S.; Netravali, A.N. Polym Compos 1999, 20, 367.
27. Reinsch, V.E.; Kelley, S.S. J Appl Polym Sci 1997, 64, 1785.
28. Dufresne, A.; Kellerhals, M.B.; Witholt, B. Macromolecules 1999, 32, 7396.
29. Dufresne, A. Compos Interfaces 2000, 7, 53.
30. Razi, P.S.; Portier, R.; Raman, A. J Composites Mater 1999, 33, 1064.
31. McCrum, N.G.; Buckley, C.P.; Bucknall, B. Principles of Polymer Engineering; Oxford University Press: New York, 1988.
32. Hashin, Z. J Appl Mech 1983, 50, 481.
33. Takayanagi, M.; Uemura, S.; Minami, S. J Polym Sci 1964, C, 5, 113.
34. Kerner, E.H. Proc Phys Soc, London 1956, 69B, 808.
35. Dickie, R.A. J Appl Polym Sci 1973, 17, 45.
36. Lewis, T.B.; Nielsen, L.E. J Appl Polym Sci 1970, 14, 1449.
37. Jourdan, C.; Cavaillé, J.Y.; Perez, J. Polym Sci Polym Phys 1989, 27, 2361.
38. Ouali, N.; Cavaillé, J.Y.; Perez, J. Plast, Rubber Compos Process Appl 1991, 16, 55.
39. Garcia-Ramirez, M.; Cavaillé, J.Y.; Dufresne, A.; Tékély, P. J Polym Sci, Polym Phys 1995, 33, 2109.
40. Garcia-Ramirez, M.; Cavaillé, J.Y.; Dufresne, A.; Dupeyre, D. J Appl Polym Sci 1996, 59, 1995.
41. Dufresne, A.; Cavaillé, J.Y.; Dupeyre, D.; Garcia-Ramirez, M.; Romero, J. Polymer 1999, 40, 1657.
42. de Gennes, P.G. Scaling Concepts in Polymer Physics; Cornell University Press: Ithaca, NY, 1979.
43. Stauffer, D. Introduction to Percolation Theory; Taylor and Francis: London, Philadelphia, 1985.
44. Focher, B.; Marzetti, A.; Conio, G.; Marsano, E.; Cosani, A.; Terbojevich, M. J Appl Polym Sci 1994, 51, 583.
45. Brandrup, J.; Immergut, E.H. Polymer Handbook, Third Edition; John Wiley & Sons, 1989.